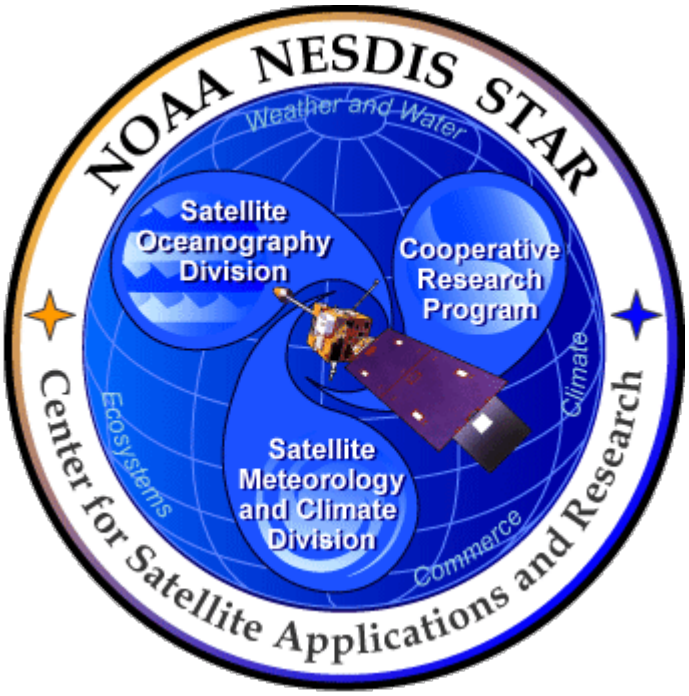


**NOAA NESDIS**
**CENTER for SATELLITE APPLICATIONS and RESEARCH**

# GOES-R Advanced Baseline Imager (ABI) Algorithm Theoretical Basis Document For Rainfall Rate (QPE)

*Robert J. Kuligowski, NOAA/NESDIS/STAR*

Version 3.0
July 10, 2020

# TABLE OF CONTENTS

# LIST OF FIGURES

# LIST OF TABLES

# LIST OF ACRONYMS

ABI – Advanced Baseline Imager
AIT – Algorithm Integration Team
AMSR2 – Advanced Microwave Scanning Radiometer 2
AMSU – Advanced Microwave Sounding Unit
ASSISTT – Algorithm Scientific Software Integration and System Transition Team
ATBD – Algorithm Theoretical Basis Document
AWG – Algorithm Working Group
BTD – Brightness Temperature Difference
CDF – Cumulative Distribution Function
CMORPH – CPC Morphing Algorithm
CPC – Climate Prediction Center
EDR – Environmental Data Record
F&PS – Functional and Performance Specification
GAS – GOES-R Archive System
GFS – Global Forecast System
GOES – Geostationary Operational Environmental Satellite
GMI – GPM Microwave Imager
GPM – Global Precipitation Measurement
GPO – GOES-R Program Office
HSS – Heidke Skill Score
IR – Infrared
LEO – Low-Earth Orbit
LHP – Loop Heat Pipe
L-U – Lower-Upper matrix decomposition
LZA – Local Zenith Angle
MIRS – Microwave Integrated Retrieval System
MWCOMB – Combined Microwave
MRD – Mission Requirements Document
MRMS – Multiple Radar Multiple Sensor
MW – Microwave
NASA – National Aeronautics and Space Administration
NCEP – National Centers for Environmental Prediction
NESDIS – National Environmental Satellite, Data, and Information Service
NOAA – National Oceanic and Atmospheric Administration
NWS – National Weather Service
OSPO – Office of Satellite and Product Operations
PDF – Probability Distribution Function
DPR – Dual-frequency Precipitation Radar
RH – Relative Humidity
SCaMPR – Self-Calibrating Multivariate Precipitation Retrieval
SEVIRI – Spinning Enhanced Visible Infrared Imager
SSMIS – Special Sensor Microwave Imager Sounder
STAR – Center for Satellite Applications and Research
QPE – Quantitative Precipitation Estimate

# ABSTRACT

This Rainfall Rate Algorithm Theoretical Basis Document (ATBD) contains a high-level description (including the physical basis) of an algorithm for estimating pixel-scale rainfall rate from images taken by the Advanced Baseline Imager (ABI) flown on the Geostationary Operational Environmental Satellite-Series R (GOES-R) series of National Oceanic and Atmospheric Administration (NOAA) geostationary meteorological satellites. A brief overview of the GOES-R observing system is followed by a more specific description of the Rainfall Rate algorithm, validation efforts, and planned improvements.

# 1 INTRODUCTION

## 1.1 Purpose of This Document

The Rainfall Rate Algorithm Theoretical Basis Document (ATBD) provides a high-level description of and the physical basis for the estimation of pixel-scale rainfall rate from images taken by the Advanced Baseline Imager (ABI) flown on the Geostationary Operational environmental Satellite-Series R (GOES-R) series of National Oceanic and Atmospheric Administration (NOAA) geostationary meteorological satellites. The rainfall rate is produced as an Environmental Data Record (EDR).

## 1.2 Who Should Use This Document

The intended users of this document are those interested in understanding the physical basis of the algorithms and how to use the output of this algorithm in a manner that is consistent with its underlying assumptions. This document also provides information useful to anyone maintaining or modifying the original algorithm.

## 1.3 Inside Each Section

This document is broken down into the following main sections.

- **System Overview**: Provides relevant details of the Rainfall Rate Algorithm and provides a brief description of the products generated by the algorithm.
- **Algorithm Description**: Provides all the detailed description of the algorithm including its physical basis, its input and its output.
- **Product Validation**: Describes the results from comparing the algorithm outputs to ground validation data sets.
- **Practical Considerations**: Provides an overview of the issues involving numerical computation, programming and procedures, quality assessment and diagnostics and exception handling.
- **Assumptions and Limitations**: Provides an overview of the current limitations of the approach and gives the plan for overcoming these limitations with further algorithm development.

## 1.4 Related Documents

This document currently does not relate to any other document outside of the specifications of the GOES-R Ground Segment Mission Requirements Document (MRD) and Functional and Performance Specification (F&PS) and to the references given throughout.

## 1.5 Revision History

Version (0.1) of this document was created by Dr. Robert J. Kuligowski of NOAA/NESDIS [National Environmental Satellite, Data, and Information Service]/STAR [Center for Satellite Applications and Research] and its intent was to serve as a draft submission to the GOES-R Program Office (GPO) for initial comments.

Version (1.0) of this document was created by Dr. Robert J. Kuligowski of NOAA/NESDIS and its intent was to accompany the delivery of the 80% algorithm to the GOES-R AWG Algorithm Integration Team (AIT).

Version (2.0) of this document was created by Dr. Robert J. Kuligowski of NOAA/NESDIS and its intent was to accompany the delivery of the 100% algorithm to the GOES-R AWG Algorithm Integration Team (AIT).

Version (3.0) of this document was created by Dr. Robert J. Kuligowski of NOAA/NESDIS and its intent was to accompany the delivery of the Enterprise version of the algorithm with the GOES-17 ABI Loop Heat Pipe (LHP) mitigation to the GOES-R AWG Algorithm Scientific Software Integration and System Transition Team (ASSISTT).

# 2 OBSERVING SYSTEM OVERVIEW

This section will describe the products generated by the ABI Rainfall Rate Algorithm and the requirements it places on the sensor.

## 2.1 Products Generated

The Rainfall Rate Algorithm produces a field of instantaneous rainfall rates associated with the most recently available GOES imagery. In terms of the F&PS, it is responsible directly for the Rainfall Rate / QPE [Quantitative Precipitation Estimate] product within the Hydrology product sub-type, and meets the requirements listed in Table 1. The Rainfall Rate Algorithm design calls for a quantitative rainfall rate in millimeters per hour on the same grid as the 2-km ABI IR bands. These products are intended for use by operational meteorologists and hydrologists for flood forecasting. There are no diagnostic products for external use aside from the official Rainfall Rate product and accompanying quality flags, but the calibration coefficient tables and rainfall class grids will be available internally for diagnostic purposes.

| **Requirement Description** | **Requirement Value** |
|---|---|
| Name | Rainfall Rate / QPE |
| User | GOES-R |
| Geographic Coverage | Full Disk |
| Temporal Coverage Qualifiers | Day and night |
| Product Extent Qualifier | Quantitative out to at least 70 degrees LZA or 60 degrees latitude—whichever is less—and qualitative beyond |
| Cloud Cover Conditions Qualifier | N/A |
| Product Statistics Qualifier | Over rain cases and mesoscale-sized surrounding regions |
| Vertical Resolution | N/A |
| Horizontal Resolution | 2.0 km |
| Mapping Accuracy | 2.0 km |
| Measurement Range | 0 – 100 mm/hr |
| Measurement Accuracy | 6 mm/hr at a rate of 10 mm/hr with higher values at higher rates |
| Product Refresh Rate / Coverage Time (Mode 3) | 15 min |
| Refreshment Rate / Coverage Time (Mode 4) | 15 min |
| Scientific Software Integration and System Transition Team | 10 min |
| Vendor Allocated Ground Latency | 266 sec |
| Product Measurement Precision | 9 mm/hr at a rate of 10 mm/hr with higher values at higher rates |

**Table 1.** F&PS Requirements for the Rainfall Rate / QPE algorithm.

Note that for pixels outside the local zenith angle and latitude cutoffs, rainfall rates will still be generated by the algorithm, but their use will be discouraged and they will not be validated for comparison against spec.

## 2.2 Instrument Characteristics

The rainfall rate is produced for each pixel observed by the ABI. Table 2 summarizes the current channel use by the Rainfall Rate Algorithm. Note that these particular bands had METEOSAT Spinning Enhanced Visible InfraRed Imager (SEVIRI) equivalents and therefore were the only ones used the original development of the algorithm prior to GOES-16 launch. ABI bands 9 and 13 have subsequently been tested in the algorithm but have not been demonstrated do have a significant positive impact on algorithm performance.

| *Channel Number* | *Wavelength (μm)* | *Resolution (km)* | *Used in Rain Rate* |
|---|---|---|---|
| 1 | 0.47 | 1.0 | |
| 2 | 0.64 | 0.5 | |
| 3 | 0.865 | 1.0 | |
| 4 | 1.378 | 2.0 | |
| 5 | 1.61 | 1.0 | |
| 6 | 2.25 | 2.0 | |
| 7 | 3.9 | 2.0 | |
| 8 | 6.19 | 2.0 | ✓ |
| 9 | 6.95 | 2.0 | |
| 10 | 7.34 | 2.0 | ✓ |
| 11 | 8.4 | 2.0 | ✓ |
| 12 | 9.61 | 2.0 | |
| 13 | 10.35 | 2.0 | |
| 14 | 11.2 | 2.0 | ✓ |
| 15 | 12.3 | 2.0 | ✓ |
| 16 | 13.3 | 2.0 | |

**Table 2.** Channel numbers, wavelengths, and footprint sizes of the ABI bands.

In addition to the data from the individual bands, the algorithm also uses brightness temperature differences (BTD's) between pairs of selected bands, and also uses some spatial gradient information from the infrared (IR) window band (14); see Section 3.4.1.2 for details. Therefore, the performance of the Rainfall Rate Algorithm is sensitive to any imagery artifacts or instrument noise. The channel specifications are given in the Mission Requirements Document (MRD) Section 3.4.2.1.4.0. The performance outlined therein was assumed during development efforts.

# 3 ALGORITHM DESCRIPTION

This section contains a complete description of the algorithm at the current level of maturity (which will improve with each revision).

## 3.1 Algorithm Overview

The rain rate algorithm identifies raining pixels and derives rain rates on a pixel level in ABI imagery. Its calibration is based on matches of ABI data with microwave (MW)-derived rainfall rates, which are considered to be the most accurate estimates of instantaneous rainfall rate available from passively-sensed satellite data. The ABI rain rate algorithm is based on the Self-Calibrating Multivariate Precipitation Retrieval (SCaMPR) algorithm first described in Kuligowski (2002) and Kuligowski et al. (2013, 2016).

After adjusting the ABI brightness temperature fields for parallax, the algorithm derives rainfall rate fields in two steps:

1. Identify pixels that are experiencing rainfall. The predictors and predictor coefficients for detecting rainfall are derived using discriminant analysis in a calibration against MW-retrieved rainfall areas.

2. Retrieve rainfall rates for pixels where rainfall has been detected. The predictors and predictor coefficients for retrieving rainfall rate are derived using linear regression and calibrated against MW-retrieved rainfall rates.

The rain rate algorithm provides estimates of instantaneous rainfall rate at the same pixel resolution as the ABI IR bands.

## 3.2 Processing Outline

The processing outline of the rain rate algorithm is summarized in Fig. 1. The rain rate is designed to run on individual pixels, with some information required from pixels in the 11x11 neighboring region.

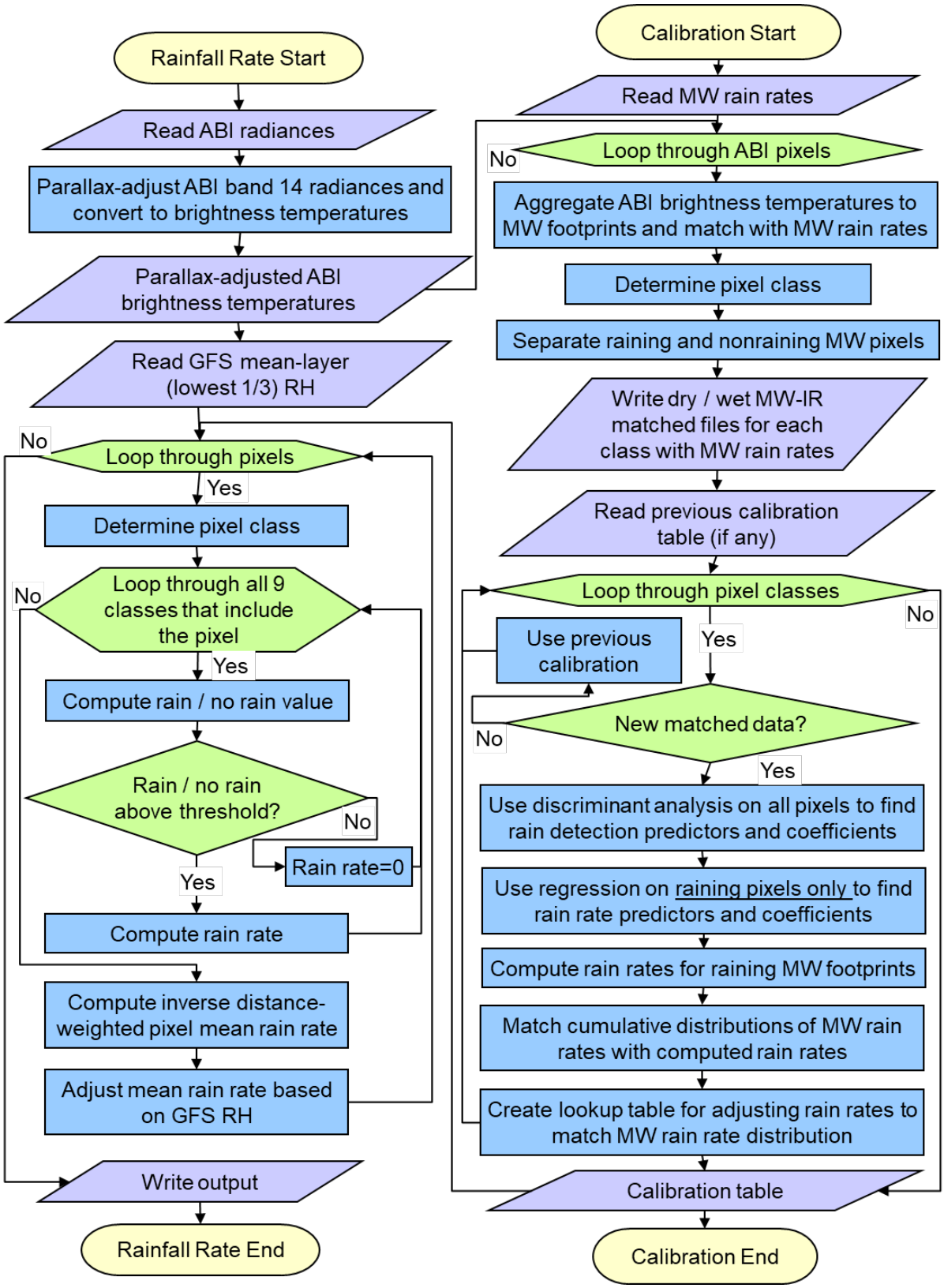


**Figure 1.** High-level flowchart of the rain rate algorithm, illustrating the main processing sections.

## 3.3 Algorithm Input

This section describes the input needed to process the rainfall rates. While the rainfall rate is derived for each pixel, it does require limited knowledge of the surrounding pixels (9x9) for rain type classification and requires band 14 from the surrounding 5x5-pixel region for two of the predictors.

### 3.3.1 Primary Sensor Data

The list below contains the primary sensor data used by the Rainfall Rate Algorithm. Primary sensor data refers to information that is derived solely from the ABI observations and geolocation information.

- Radiances for channels 8, 10, 11, 14, and 15
- Pixel latitude, longitude, and local zenith angle (LZA)
- Any relevant ABI quality control flags

### 3.3.2 Ancillary Data

The following list briefly describes the ancillary data requited to run the Rainfall Rate Algorithm. Ancillary data is defined as data that requires information not included in the ABI observations or geolocation data. All five of these ancillary data sets would be considered to be non-ABI dynamic data (i.e., they are not other ABI-derived products); no static ancillary data (i.e., time-constant ancillary data such as topography or a land/sea mask) are required.

- **Numerical model fields of temperature and geopotential height**

  Fields of temperature and geopotential height from the NOAA / National Weather Service (NWS) / National Centers for Environmental Prediction (NCEP) Global Forecast System (GFS) are used to estimate cloud-top heights from the limb-adjusted ABI band 14 brightness temperatures to adjust the pixels for parallax. These fields are currently at 0.25° lat / lon resolution and are for 26 pressure levels from 1000 – 10 hPa. To account for the time lag between the initialization time and the availability of the forecast files, the GFS forecast lead times from 6 to 11 hours from the most recent forecast run are used.

- **Numerical model fields of relative humidity (RH)**

  Mean-layer RH is computed for the lowest third of the GFS model domain on the same grid and for the same lead times as for the temperature and geopotential height. These values are used to adjust the retrieved rainfall rates for the effects of evaporation below cloud base.

- **MW-derived rainfall rates**

  Rainfall rates, presumably from MW data but also permissible from active radar, are required as a calibration target for the algorithm. These rainfall rates do not need to be available in real time, though the accuracy of the rain rate estimates tends to degrade as the difference between the time period covered by the training data and the time of the retrieval from the ABI becomes longer. The MW rainfall rates are currently from the NOAA / NWS / Climate Prediction Center (CPC) combined microwave (MWCOMB) field, which is an intermediate product from the CPC Morphing (CMORPH) algorithm (Joyce et al. 2004). Each hourly MWCOMB file contains two half-hourly grids of intercalibrated MW rain rates remapped to a common ~0.073° lat / lon grid. Efforts are underway to directly match the IR data in real time from microwave rain rates; see Section 6.3.1 for additional details.

- **Matched MW rain rates and ABI predictors**

  These MW-derived rainfall rates are matched with ABI-derived predictors that have been aggregated to the MWCOMB grid (0.073° lat / lon), multiplied by 100, and written to a netCDF4 file. Each data point containing non-missing MWCOMB data is stored in an integer*2 array called Matched_DataSet with dimensions Param_Num, Rec_Num) where Param_Num is the total number of matched data points in the file and Param_Num is 10. The values corresponding to the 10 entries are given in Table 3:

| Element | Variable | Value |
|---|---|---|
| 1 | MW pixel latitude (degrees * 100, north positive) | -6000 to 6000 |
| 2 | MW pixel longitude (degrees *100, east positive) | -18000 to 18000 |
| 3 | MW rainfall rate (mm/h * 100) | 0 to 5000 |
| 4 | ABI band 8 brightness temperature (K * 100) | 17400 to 32500 |
| 5 | ABI band 10 brightness temperature (K* 100) | 17400 to 32500 |
| 6 | ABI band 11 brightness temperature (K* 100) | 17400 to 32500 |
| 7 | ABI band 14 brightness temperature (K* 100) | 17400 to 32500 |
| 8 | ABI band 15 brightness temperature (K* 100) | 17400 to 32500 |
| 9 | $S = 0.568*(T_{min,11.2}-217\ K) * 100$ | -10743 to 4357 |
| 10 | $G_t = T_{avg,11.2} - T_{min,11.2} * 100$ | 0 to 15100 |

**Table 3.** Contents of each data record of the IR-MW matched data file.

In Table 3, $T_{min,11.2}$ is defined as the minimum band 14 brightness temperature in a 5x5-pixel box centered on the pixel of interest and $T_{avg,11.2}$ is the average band 14 brightness temperature for the 2 pixel on either side and the 1 pixel above and below the pixel of interest; see Ba and Gruber (2001) for details.

- **Retrieval coefficient table**

  The retrieval coefficient table file contains the ID's (from the matched file) of the selected predictors along with their calibration coefficients for both rain / no rain discrimination and rain rate calibration which are stored in a netCDF4 file. A list of the contents of this file is provided in Table 4, followed by the definition of the dimension constants.

| Name | Description | Type(dimension) |
|---|---|---|
| HSS | Heidke Skill Score of rain / no rain discrimination for calibration data | real*4(Class_Num) |
| Corr_Coeff | Pearson Correlation Coefficient of (untransformed) rain rate for calibration data | real*4(Class_Num) |
| ID_Predictor | Predictor IDs of rain rate predictors 1 and 2 and of rain / no rain predictors 1 and 2 | int*4 (Class_Num, AllPredictor_Num) |
| AmountParam | Rain rate calibration intercept and multipliers for rate predictors 1 and 2 | real*8 (Class_Num, MaxPredictor_Num+1) |
| DiscrimParam | Rain / no rain calibration multipliers for rain / no rain predictors 1 and 2 | real*8 (Class_Num, DisPredictor_Num) |
| Thresh_Rain | Rain / no rain threshold | real*4 (Class_Num) |
| ParamA_Transform | Nonlinear transformation multiplier for rain rate predictors 1 and 2 | real*8 (Class_Num, MaxPredictor_Num) |
| ParamB_Transform | Nonlinear transformation exponent for rain rate predictors 1 and 2 | real*8 (Class_Num , MaxPredictor_Num) |
| Deltax_Transform | Nonlinear transformation intercept for rain rate predictors 1 and 2 | real*8 (Class_Num, MaxPredictor_Num) |
| AdjLUT | LUT for adjusting rain rain rates to match MW distribution | real*4 (Class_Num, LUTBin_Num) |

**Table 4.** Contents of the retrieval coefficient table file.

The dimension constants in the retrieval coefficient table file are defined as follows:

- Class_Num (number of algorithm classes) = 330 for GOES-16; 440 for GOES-17 (see Section 3.4.2)
- AllPredictor_Num (total number of selected predictors) = 4
- MaxPredictor_Num (number of selected rain rate predictors) = 2
- MaxPredictor_Num+1 (number of selected rain rate predictors + 1) = 3
- DisPredictor_Num (number of selected rain / no rain predictors) = 2
- LUTBin_Num (number of LUT bins used for the rate adjustment) = 10000

## 3.4 Theoretical Description

As stated previously, retrieval of rainfall rate requires two steps: determining which pixels in satellite imagery will be associated with rainfall, and then deriving rainfall rates

for those pixels. In the case of visible / IR instruments such as the ABI, the basic approach is to use the information about cloud-top properties that are inherent in the brightness temperature information (e.g., height, thickness, phase, particle size) to make inferences about the occurrence and intensity of rainfall. This algorithm develops statistical relationships between the brightness temperature values and the occurrence of rainfall and its intensity. In the algorithm, discriminant analysis is used to determine the best predictors and predictor coefficients for occurrence, and linear regression is used for intensity.

### 3.4.1 Physics of the Problem

The difficulty in using visible- and IR-wavelength information for retrieving rainfall rates is that raining clouds are generally optically thick, meaning that the information at these wavelengths comes from the top portion of the cloud, and typically above precipitating hydrometeors that are actually of interest. MW-frequency information is relatively more valuable because raining clouds are generally not optically thick in that portion of the spectrum, meaning that MW signals are sensitive to the total water or ice path in the cloud rather than just the properties of the cloud top. However, since MW sensors are for the near future restricted to low-Earth orbit (LEO), rainfall information from such instruments will not be available on a continuous basis without a much more substantial LEO satellite constellation than is currently planned. The compromise has been to use the intermittently-available but relatively more accurate MW-based rainfall rates as a calibration target for IR data from geostationary platforms, and to use the resulting calibration to retrieve rainfall rates at the full spatial and temporal resolution of the geostationary data.

On a more fundamental level, location errors of clouds caused by parallax can degrade the relationship between the IR data and the MW rain rates and can also reduce the skill of the rainfall rate retrievals that are based on the IR data. An adjustment for parallax is applied during the initial step of IR processing to reduce these errors.

The following subsections describe how these processes are performed in additional detail. The first subsection describes the parallax adjustment since it is the initial step in the process. The second subsection describes the MW data set that is used as a calibration target and how it is matched against the ABI predictors, and the subsequent four subsections describe respectively how the training data are assembled, how the rainfall detection algorithm is calibrated, how the Rainfall Rate Algorithm is calibrated, and then how the resulting calibration is applied to independent data to product the rain rate product.

#### 3.4.1.1 Parallax Adjustment

The location of a surface or atmospheric feature in a satellite image is dependent upon three factors: the actual location of the feature, the location of the satellite observing point, and the deviation in height of the feature from the assumed surface that is used for geolocation of the satellite pixels. These can be related to the apparent location of the

feature in satellite imagery using relatively simple geometric relationships that will be described in detail in Section 3.5.1.

#### *3.4.1.1.1 Height Determination*

To determine the cloud-top height, the GFS temperature and height profiles are interpolated from the four nearest GFS grid points to the center of the ABI pixel, and then the ABI band 14 (11.2-μm) brightness temperature $T_{11.2}$ is compared to this profile. This method assumes that the cloud is optically thick, which is satisfied for clouds that are thick enough to produce rainfall.

Using this method also requires that limb darkening be accounted for (i.e., to avoid excessively high cloud-top height retrievals). The climatological adjustment for limb darkening developed by Joyce et al. (2001) is applied to ABI band 14 before using them to derive the cloud-top height. It should be noted that the limb-adjusted brightness temperatures are not used in the calibration or retrieval process, since a climatological adjustment is inappropriate for WV absorption bands. It should also be noted that even at nadir the IR bands experience a small amount of attenuation from WV absorption, which in turn could cause the cloud-top height assignment to be slightly too high. However, since the cloud-top height is being used to compute a parallax adjustment with a minimum resolution of 2 km (the distance between footprints at nadir), an error in the height assignment of even a few hundred meters can be ignored for this application.

#### *3.4.1.1.2 Location Adjustment*

For each pixel in the ABI image, a pre-computed LUT contains the pixel location to which it should be shifted based on the cloud-top height. This LUT is used to shift the pixels in each of the IR bands, and any gaps in the field of shifted IR pixels is filled in using simple inverse-distance-weighted interpolation.

### 3.4.1.2 Training Data: Matched ABI Predictors and Microwave Rain Rates

The MW rain rates serve as the calibration target for the rain rate algorithm, both in terms of identifying raining areas and in retrieving the intensity of rainfall. In practice, any reliable rainfall rate field could be used for calibration, including radar data, and it is not necessary that these fields be continuous in space or time—just that they represent instantaneous rates of rainfall rather than accumulations over time. Since rainfall rates from multiple microwave instruments are used, the rates should be bias-adjusted since differences among the input data sets will effectively act as noise in the training data set. This was the motivation behind the initial choice to calibrate against the MWOMB product..

To properly match the ABI predictors with the MW rain rates in space, differences in footprint size between the ABI and the MW sensors must be addressed. The procedure in this algorithm is to aggregate the ABI data onto the MWCOMB grid. Although the satellite contributing to a particular MWCOMB grid point is known, the size of the

original MW footprint is not known for cross-track scanning instruments like the AMSU-B / MHS and can only be inferred from the original swath data. Consequently, it is assumed that the MW footprint is 8 km (an approximation of the MWCOMB grid size). Furthermore, it is also assumed that the ABI footprint diameter is 2 km even though it is known that the ABI footprint size varies with scan angle. For each available MW footprint, those ABI footprints that at least partially overlap the MW footprint are identified, and the fraction of the coverage of the MW footprint by the ABI footprint is computed based on the location of the footprint centers and the above assumptions about footprint shape and size. The weight of each ABI footprint is proportional to the total computed overlapping area with the MW footprint such that all of the weights add up to unity.

Time matching of the ABI predictors with the MW rain rates should match the ABI and MW fields that are closest in time. Since the MWCOMB fields contain all of the MW overpasses during a 30-min period with no time information, the ABI fields to match are arbitrarily taken from those ABI scans that start at the beginning of each MWCOMB field. Due to the 15-h latency of MWCOMB, previous ABI images will need to be available for matching with microwave data.

Note that the predictors in this algorithm are not necessarily restricted to ABI data; predictors from other GOES-R instruments (e.g., lightning) can also be used, in addition to any other ancillary data that might prove to be relevant (e.g., stability profiles from numerical weather models). The current list of predictors is presented in Table 5, where the subscript refers to the wavelength of the brightness temperature T; e.g., $T_{7.34}$ is the brightness temperature at 7.34 μm. Note that the matched MW-ABI data file contains the component IR brightness temperature values and also the derived values in Predictors 2 and 3; the additional predictors in Table 5 (i.e., brightness temperature differences) are computed internally by the calibration program to reduce the required size of the matched data files. The constant adjustments are performed in order to optimize the nonlinear predictor transformation described in Section 3.5.4. In the case of brightness temperature differences, a constant is added in order to avoid negative values which have an undefined logarithm; in the case of the brightness temperature values, a constant is subtracted because lower (but positive) values are most sensitive to the nonlinear transformation.

| **Input ID** | **Description** |
|---|---|
| 1 | $T_{6.2}$ - 174 K |
| 2 | $S = 0.568*(T_{min,11.2}-217\ K) + 25\ K$ |
| 3 | $T_{avg,11.2} - T_{min,11.2} - S + 85\ K$ |
| 4 | $T_{7.34} - T_{6.19} + 10\ K$ |
| 5 | $T_{8.5} - T_{7.34} + 10\ K$ |
| 6 | $T_{11.2} - T_{7.34} + 40\ K$ |
| 7 | $T_{8.5} - T_{11.2} + 25\ K$ |
| 8 | $T_{11.2} - T_{12.3} + 15\ K$ |
| 9 | $T_{11.2}$ - 174 K |

| | |
|---|---|
| 10-18 | Nonlinear transformations of predictors 1-9 |

**Table 5.** Predictors computed from the data in the matched MW-ABI data file.

Note that if a particular pixel is present but there are missing pixels in the 5x5 neighboring region, $T_{min}$ (and hence S) will still be computed, but the missing pixels will be ignored in calculating the predictors that require information from the neighboring region. However, if at least 3 of the 6 neighboring pixels (the closest 4 in the same scan line and the 2 corresponding pixels in the adjacent scan lines) used to compute $G_t$ are missing $G_t$ is not computed and is assigned a missing value of -999.0.

Finally, if any of these predictors has a value less than or equal to zero, the nonlinear transformation (see Section 3.5.4) cannot be performed and so no retrieval is performed for such pixels; their rainfall rate value is set to a missing value of -999.0.

The performance of the rain rate algorithm has been shown to improve when the data are divided into classes that can be determined a priori from available data. Specifically, the ABI full disk is divided into 15x15° lat / lon boxes, as shown in Fig. 2:

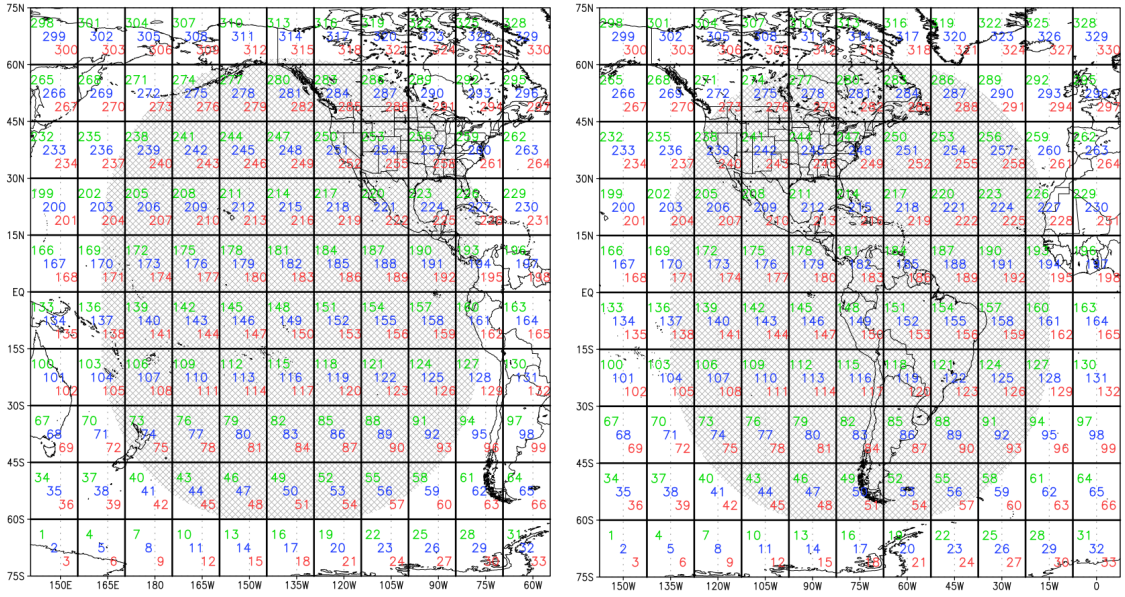

**Figure 2.** Calibration boxes for GOES-West (left) and GOES-East (right). Green values are for water-top clouds; blue values are for ice-top clouds; and red values for deep-convective clouds. Cross-hatching indicates the region with a satellite zenith angle of < 70°; i.e., the region of quantitative validation.

In addition, the data in each box are divided into 3 rainfall types according to selected ABI brightness temperature values from the matched MW-ABI data set that are computed for the 9x9-pixel window centered on the pixel of interest in order to produce a spatially smooth cloud type field:

– Type 1 (water cloud): $T_{7.34}<T_{11.2}$ and $T_{8.5}-T_{11.2}<-0.3$

- Type 2 (ice cloud): $T_{7.34} < T_{11.2}$ and $T_{8.5} - T_{11.2} \geq -0.3$
- Type 3 (cold-top convective cloud): $T_{7.34} \geq T_{11.2}$

These types were determined by experimenting with the changes in the relationship between $T_{11.2}$ and rainfall rate ($T_{11.2}$ is the band typically used for rain rate retrievals because of its sensitivity to cloud-top temperature with relatively small water vapor effects) for various brightness temperature threshold difference regimes. The thresholds are the points at which this relationship changes significantly from one side of the threshold to the other, which implies that they represent significantly different regimes for rainfall rate retrieval purposes. This results in a total of 330 rainfall classes in the algorithm (440 for GOES-17; see Section 3.4.2) which are illustrated in Fig. 2. Separate files of matched MW rain rates and ABI data are maintained for each class.

Note also that if any of the three ABI brightness temperature values used to determine cloud type ($T_{7.34}$, $T_{8.5}$, or $T_{11.2}$) is missing for a given pixel, the rainfall class will be set to zero and no retrieval will be performed for that particular pixel (i.e., its value will be set to -999.0).

Separate matched data sets are maintained for each rainfall class, with the data points in reverse time order (i.e., the most recent data in the first record and the oldest data in the last record). These matched data sets are rolling-value data sets; i.e., older data are cycled out of the end of the file as newer data are brought in to the beginning of the file keep the data set up-to-date. Initial work with training data sets covering a fixed period of time (e.g., 24 hours) proved to be unsuitable because time variations in the intensity distribution of rainfall would affect the robustness of the calibration. For example, if an extended period of light rain or no rain were followed by heavy rain, the algorithm might be preferentially calibrated for light rain and thus perform poorly when the heavy rain began. To ensure a training data set that contains enough raining pixels for reliable results but is still short enough to reflect recent conditions, the number of data points with MW rain rates > 2.5 mm/h in the training data files are kept fixed at 10,000. Specifically, as newer data become available and are added to the training data file, the oldest data points are removed until the number of MW pixels with rain rates > 2.5 mm/h returns to the same value as before the newer data were added. It should be noted that the number of training pixels read is controlled by the training code rather than by the file size; i.e., the training code will read through the training file (backward in time) until the required number of raining pixels is read. Therefore, it is not critical for the training file to be trimmed strictly to the required number of training pixels as extra pixels will simply be ignored.

It is important to note that the training of the coefficients and the retrieval of the actual rain rates are done in parallel: the coefficients are updated whenever new target data become available, and then these updated coefficients are used in retrieving the rain rates from the next available set of ABI imagery.

### 3.4.1.3 Rainfall Detection

The objective of the rainfall detection portion of the algorithm is to separate clear and cloudy but non-raining pixels from raining pixels. The training of the separation portion of the algorithm is applied to each cloud class separately using discriminant analysis (similar to linear regression but with a binary predictand—the value is 1 if the MW rain rate exceeds 1.0 mm/h and 0 otherwise. The 1.0 mm/h threshold is used because of significant differences among MW instruments in sensitivity to drizzle and very light rain). For each algorithm class, discriminant analysis is performed using each possible predictor pair, and the pair that produces the best Heidke Skill Score (HSS; see Section 3.5.3 for definition) for rain / no rain discrimination (compared to observations) is selected. The result is an equation for linearly combining two predictors, plus a threshold value above which the pixel is considered to be raining. This threshold value is optimized based on the Heidke Skill Score (HSS) but with the constraint that the retrieved and actual number of raining pixels cannot differ by more than 5%.

Once the predictors and coefficients have been selected and the threshold value has been determined, the resulting predictor ID's and coefficients are then written to a file for use by the prediction program. A more detailed description of this process is contained in Section 3.5.3.

### 3.4.1.4 Rainfall Rate Estimation

The objective of the rainfall rate portion of the algorithm is to determine rainfall rates for those pixels that were classified as raining by the discriminant analysis scheme, with separate equations for each algorithm class. Consequently, only those pixels that have non-zero target rainfall rates are used to develop the equations for retrieving rainfall rates.

Since the relationship between many of the predictors (e.g., IR window brightness temperature) and rainfall rates is known to be nonlinear, the first step is to supplement the predictor set with additional predictors that represent optimal nonlinear transformations of the original set: for each algorithm class, each original predictor is re-scaled to eliminate negative values (see Table 5), and then the predictors and target rain rates are regressed against each other in $\log_{10}$-$\log_{10}$ space. The resulting slope and intercept become an exponent and multiplier in linear space, and this slope and intercept are used to create a nonlinear transformation of each predictor.

After creating the set of transformed predictors for each algorithm class (which are included with the original predictors in the predictor pool), all of the possible predictor pairs are evaluated via linear regression against the target rain rates, with separate regressions performed for each algorithm class. The predictor pair that produces the best correlation with the target rain rates is selected. After this is done, a preliminary set of rain rates is retrieved and compared to the MW training data to derive a set of coefficients for adjusting the retrieved rain fall rate distribution to match the distribution of the microwave rainfall rates. All of the required coefficients are then written to a file for use

by the prediction routine. A more detailed description of this process is contained in Section 3.5.4.

#### 3.4.1.5 Independent rainfall rates

The equations produced by the calibration of the rainfall detection and rainfall rate estimation are used to derive the rainfall rates from current ABI imagery that comprise the algorithm output at the full ABI resolution. For each pixel, the rain / no rain and rain rate equations for that pixel's cloud type for the 3x3 15° lat / lon boxes centered on the pixel. Note that the rainfall rates are produced using different equations for each of the 330 (440) classes.

### 3.4.2 GOES-17 ABI LHP Issues and Mitigation

It was discovered during post-launch testing of the GOES-17 ABI that the loop heat pipe (LHP) subsystem, which transfers heat from the ABI electronics to the radiator, is not operating at its designed capacity. Because of this, the ABI Focal Plane Module (FPM) cannot be maintained at their intended temperatures, which makes the infrared imagery noisier than spec and also leads to partial loss of imagery during some of the overnight hours before and after the vernal and autumnal equinoxes. For additional details, please refer to https://www.goes-r.gov/users/GOES-17-ABI-Performance.html.

Some strategies have been employed to mitigate the effects of the LHP issue, including a modified calibration method to reduce the biases caused by changes in the FPM temperature. In addition, a modified GOES-17 ABI scan schedule is used during the warmest periods whereby full disk images are taken every 15 min and no CONUS sectors are scanned in order to allow the FPM to be turned away from the sun and cool down slightly; this has reduced the heating by a few degrees K.

However, while the noise is manageable in the individual bands when the FPM is not heating up, the noise in the BTDs is much more noticeable since the signal in a BTD is much weaker than in an individual band. Since the Enterprise Rainfall Rate algorithm relies so heavily on BTDs (see Table 5), and since it has been demonstrated elsewhere that this noise was causing the retrieved rain rates to be quite noisy, it was decided to only use band 14 for GOES-17 retrievals regardless of the FPM temperature, which made predictors 2, 3, and 9 from Table 5 the only ones in the predictor pool. These changes are discussed in more detail in Section 3.5.6.

## 3.5 Mathematical description

### 3.5.1 Calculation of the location shift

As outlined in Vicente et al. (2002), three inputs are required for parallax correction:

- Cloud (or feature) height $H_c$,
- Apparent position on the Earth of the feature (latitude $\theta_c$, longitude $\varphi_f$)

- Satellite position (distance $R_s$ from the center of the earth over a sub-point at latitude $\theta_s$ and longitude $\varphi_s$)

If the surface of the Earth is considered to be an ellipsoid with an equatorial radius of $R_{equator}$ = 6378.1 km and a polar radius $R_{pole}$ of 6356.6 km, then it can be represented by the following equation:

$$\left(\frac{X}{R_{equator}}\right)^2 + \left(\frac{Y}{R_{pole}}\right)^2 + \left(\frac{Z}{R_{equator}}\right)^2 = 1. \quad (1)$$

Assuming a Cartesian coordinate system where the x-axis of this ellipsoid Earth runs through the intersection of the Equator and Prime Meridian, that the y-axis runs through the poles, and that the z-axis is positive through the Equator at a latitude of 90 degrees East, the distance of the surface of this ellipsoid from its center $R_e$ as a function of latitude and longitude is

$$R_e = \frac{R_{equator}}{\cos^2\theta_c + \left(\frac{R_{equator}}{R_{pole}}\right)^2 sin^2\theta_c} \quad (2)$$

With this information, the apparent position of the cloud on the Earth's surface (i.e., at distance $R_e$ from the Earth's center) can be expressed in Cartesian coordinates ($X_c$, $Y_c$, $Z_c$) as follows:

$$X_c = R_e \cos\theta_c \, sin\varphi_c \quad (3)$$

$$Y_c = R_e \, sin\theta_c \quad (4)$$

$$Z_c = R_e \cos\theta_c \, cos\varphi_c \quad (5)$$

The location of the satellite ($X_s$, $Y_s$, $Z_s$) can be likewise stated in Cartesian coordinates, substituting the s subscript for c in the above equations. However, for a satellite in geostationary orbit, $\theta_s$=0 and thus $Y_s$ = 0.

Since the actual position of the cloud in Cartesian coordinates ($X_a$, $Y_a$, $Z_a$) lies on the line that connects the apparent position of the cloud on the Earth's surface ($X_c$, $Y_c$, $Z_c$) and the satellite ($X_s$, $Y_s$, $Z_s$), the actual position of the cloud can be expressed in terms of the other two positions as

$$X_a = X_c + A(X_s - X_c) \quad (6)$$

$$Y_a = Y_c + A(Y_s - Y_c) \quad (7)$$

$$Z_a = Z_c + A(Z_s - Z_c) \quad (8)$$

Determining the scaling factor A will enable determination of the actual cloud location. Applying the same ellipsoid equation to the height of the feature above the surface $H_c$ gives the result

$$\left(\frac{X_a}{R_{equator}+H_c}\right)^2+\left(\frac{Y_a}{R_{pole}+H_c}\right)^2+\left(\frac{Z_a}{R_{equator}+H_c}\right)^2=1, \quad (9)$$

and substituting Eq. (6)-(8) and then Eq. (3)-(5) into Eq. (9) followed by reorganizing and simplifying results in a second-degree equation on A that has the following solution:

$$A=\frac{-D+\sqrt{D^2-4CE}}{2C} \quad (10)$$

where C, D, and E are defined as

$$C=(X_s-X_c)^2+(Z_s-Z_c)^2+B(Y_s-Y_c)^2 \quad (11)$$

$$D=2[X_c(X_s-X_c)+Z_c(Z_s-Z_c)+BY_c(Y_s-Y_c) \quad (12)$$

$$E=X_c^2+Z_c^2-\left(R_{equator}+H_c\right)^2+BY_c^2 \quad (13)$$

and B is further defined as

$$B=\left[\frac{R_{equator}+H_c}{R_{polar}+H_c}\right]^2. \quad (14)$$

Once the actual cloud Cartesian coordinates ($X_a$, $Y_a$, $Z_a$) have thus been obtained, the actual latitude $\theta_a$ and longitude $\varphi_a$ of the feature can be determined by

$$\theta_a=\arctan\left[\frac{Y_a}{\sqrt{X_a^2+Z_a^2}}\right] \quad (15)$$

$$\varphi_a=\arctan\left[\frac{X_a}{Z_a}\right] \quad \text{if } Z_a>0 \quad (16)$$

$$\varphi_a=\arctan\left[\frac{X_a}{Z_a}\right]-180° \quad \text{if } Z_a<0 \quad (17)$$

$$\varphi_a=90° \quad \text{if } Z_a=0 \text{ and } X_a>0 \quad (18)$$

$$\varphi_a=-90° \quad \text{if } Z_a=0 \text{ and } X_a<0 \quad (19)$$

As stated previously, instead of computing the parallax correction each time, a LUT is created once that contains the parallax shifts for selected ranges of cloud-top brightness temperature, and this is what is used in the real-time parallax correction process.

### 3.5.2 ABI-MWCOMB matching

The starting point for matching the ABI and MWCOMB footprints is to determine the distance between the centers of the two. The assumption of a spherical Earth (since the distances involved are less than 20 km) leads to the equation

$$Distance = \{[(lon_{ABI} - lon_{MW}) * \cos(lat_{MW})]^2 + [(lat_{ABI} - lat_{MW})]^2\} * 111\ km \quad (20)$$

where $lat_{ABI}$ and $lat_{MW}$ are the latitudes of the centers of the ABI and MW footprints, and $lon_{ABI}$ and $lon_{MW}$ are the corresponding longitudes. Presuming the distance is less than the sum of the two radii ($r_{ABI}$=1 km, $r_{MW}$=4 km; both footprints assumed to be perfect circles), so that the two circles have a common area. Two possible scenarios exist in that case: if the distance is less than the radius of the smaller (ABI) radius, then the ABI footprint is contained entirely within the MW footprint and so the common area is simply the ABI footprint area ($\sqcap r^2_{ABI}$). If the distance is greater than the ABI radius but smaller than the sum, then the common area of the two circles is expressed as

$$Area = r_{MW}^2 * (\alpha - \cos(\alpha)\sin(\alpha)) + r_{ABI}^2 * (\beta - \cos(\beta)\sin(\beta)) \quad (21)$$

where

$$\alpha = acos\left[\frac{-r_{ABI}^2 + distance + r_{MW}^2}{2 * r_{MW}^2 * distance}\right] \quad (22)$$

and

$$\beta = asin\left[\frac{r_{MW} * \sin(\alpha)}{r_{ABI}}\right] \quad (23)$$

and

$$\beta = \pi - \beta \text{ if distance} < r_{MW}\cos(\alpha) \quad (24)$$

The weight of each ABI pixel in computing the MW value is simply the common area of the ABI and MW pixel divided by the total area of ABI pixels within the MW pixel; thus, the weights for each MW pixel always add up to unity. In other words, for each ABI pixel i among a total of n ABI pixels (or partial pixels) within the MW pixel of interest, the weight $w_i$ is computed as

$$w_i = \frac{Area_i}{\sum_{i=1}^{n} Area_i} \quad (25)$$

### 3.5.3 Calibration: Rain / no rain discrimination

Mathematically, a special case of multiple linear regression called discriminant analysis (in which the target values are 0 for rain rates < 1 mm/h and 1 otherwise instead of continuous values) is used to separately calibrate the rain /no rain discrimination for each algorithm class. A two-predictor additive multiple regression model is used for each algorithm class *c*:

$$y_c = b_{c,0} + b_{c,1}x_{c,1} + b_{c,2}x_{c,2} + \varepsilon_c \quad (26)$$

where y is the target MW rain rate or rain / no rain value; the x's are the two selected ABI-derived predictors; the b's are the calibration coefficients; and ε is the residual error, which is to be minimized by solving the following system of normal equations for the coefficients $b_0$, $b_1$, and $b_2$:

$$\begin{aligned}
\sum_{j=1}^{n_c} y_{c,j} &= b_{c,0} n_c + b_{c,1} \sum_{j=1}^{n_c} x_{c,1,j} + b_{c,2} \sum_{j=1}^{n_c} x_{c,2,j} \\
\sum_{j=1}^{n_c} x_{c,1,j} y_{c,j} &= b_{c,0} \sum_{j=1}^{n_c} x_{c,1,j} + b_{c,1} \sum_{j=1}^{n_c} x_{c,1,j}^2 + b_{c,2} \sum_{j=1}^{n_c} x_{c,1,j} x_{c,2,j} \\
\sum_{j=1}^{n_c} x_{c,2,j} y_{c,j} &= b_{c,0} \sum_{j=1}^{n_c} x_{c,2,j} + b_{c,1} \sum_{j=1}^{n_c} x_{c,1,j} x_{c,2,j} + b_{c,2} \sum_{j=1}^{n_c} x_{c,2,j}^2
\end{aligned} \tag{27}$$

where the first part of the subscript is the algorithm class, the second is the predictor number, and the third part is the data point number (all sums are over the total number of data points in the class $n_c$.)

The calibration procedure begins by solving these equations for each possible pairing of the first 9 (untransformed) predictors in the matched data set (see Table 5). Since the outputs of these equations will be continuous (i.e., non-binary), a threshold value must be determined for converting the output to binary values: outputs above the threshold are assigned a value of 1 (rain) and outputs below are assigned a value of 0 (no rain). This threshold is selected to produce the maximum skill (as measured using the Heidke Skill Score; see Eq. (28)) with the constraint that the bias ratio must be between 0.95 and 1.05; i.e., there can be no more than a 5% difference between the number of pixels in the training data set that are classified as raining and the actual number of raining microwave pixels in the training data set. In order to do this, the equation outputs are computed for each training pixel and the highest and lowest values are preserved. This range of values is divided into 5,000 equally spaced intervals, and for each of these 5,000 threshold values the number of pixels classified as raining is computed. Since this number decreases monotonically as the threshold value increases (the threshold value must be exceeded), a simple binary search can then be used to identify the threshold value that produces the best match to the microwave data in terms of the number of raining pixels.

The HSS is computed as follows:

$$HSS = \frac{2(c_1 c_4 - c_2 c_3)}{(c_1 + c_2)(c_2 + c_4) + (c_3 + c_4)(c_1 + c_3)} \tag{28}$$

where $c_1$ is the number of correct no-rain estimates, $c_2$ is the number of false alarms (i.e., the estimate has rain but the observation has no rain); $c_3$ is the number of failed detections (i.e., the estimate has no rain but the observation has rain); and $c_4$ is the number of correct rain estimates for the class of interest. Higher HSS values indicate greater skill, with 1 as a perfect value (i.e., $c_2$=$c_3$=0).

It should be noted that the selection of only 2 predictors was the result of experimentation: additional predictors were shown not to have a positive impact on the performance of the algorithm. This may be due to the high degree of correlation among the IR bands when depicting optically thick clouds.

### 3.5.4 Calibration: Rainfall rate

For each class, a separate pair of predictors is selected for the rain rate retrieval, using Eqs. (26)-(27) as the basis for selection but with continuous output. Prior to selection, the set of 9 predictors is supplemented by a set of non-linear transformations (see Table 5). These nonlinear transformations for each predictor $p$ and class $c$ $x_{p,c}^T$ use the power function; i.e.,

$$x_{p,c}^T = \alpha_{p,c} x_{p,c}^{\beta_{p,c}} \tag{29}$$

where the coefficients $\alpha_{p,c}$ and $\beta_{p,c}$ are found by solving the equation

$$\log_{10} y = \log_{10} \alpha_{p,c} + \beta_{p,c} \log_{10} x^T . \tag{30}$$

Solving this equation separately for each predictor and class yields the following least-squares solutions:

$$\beta_{p,c} = \frac{n_{p,c} \sum_{i=1}^{n_{p,c}} \left(\log_{10} x_{p,c,i}\right)\left(\log_{10} y_{c,i}\right) - \sum_{i=1}^{n_{p,c}} \left(\log_{10} x_{p,c,i}\right) \sum_{i=1}^{n_{p,c}} \left(\log_{10} y_{c,i}\right)}{n_{p,c} \sum_{i=1}^{n_{p,c}} \left(\log_{10} x_{p,c,i}\right)^2 - \left(\sum_{i=1}^{n_{p,c}} \log_{10} x_{p,c,i}\right)^2} \tag{31}$$

$$\log_{10} \alpha_{p,c} = \frac{\sum_{i=1}^{n_{p,c}} \left(\log_{10} y_{c,i} - \log_{10} x_{p,c,i}\right)}{n_{p,c}} \tag{32}$$

For each predictor $p$ in each class $c$, the coefficients $\alpha_{p,c}$ and $\beta_{p,c}$ are solved for by applying Eq. (31) and (32) using the predictor values $x_{p,c,i}$ and the corresponding target microwave rainfall rates $y_{c,i}$. However, since the equation form in Eq. (29) has no intercept, it would be constrained to pass through the origin (0,0), so a modified version was developed.

$$x_{p,c}^T = 10^{\alpha_{p,c}} \left(x_{p,c} + 1 + \gamma_{p,c}\right)^{\beta_{p,c}} - 1 \tag{33}$$

The third unknown ($\gamma_{p,c}$) cannot be solved for with only two equations, so the equation is optimized using a "brute force" approach. First, the value of $\gamma_{p,c}$ is initially set to 0 and the equation is solved using Eq. (31) and (32). The value of $\gamma_{p,c}$ is then incremented by 25 and Eq. (31) and (32) are solved again; i.e., the value of $\gamma_{p,c}$ is added to the each

predictor value $x_{p,c}$ when solving the equation. The Pearson correlation coefficient is then computed for the transformed data:

$$Correlation = \frac{\mathrm{cov}(x, y)}{\sigma_x \sigma_y} \tag{34}$$

where cov(x,y) is the covariance of the predictor and target data, and $\sigma_x$ and $\sigma_y$ represent the standard deviations of the predictor and target data, respectively. The predictor data in this case consists of the values of the transformed predictors (i.e., $x^T_{p,c}$) and the target data consist of the MW rainfall rates against which they have been matched (i.e., $y_c$).

If the equation fit (as measured by correlation coefficient) is improved, the value of $\gamma_{p,c}$ is incremented by 25 and the process is repeated (but is stopped if it reaches 2500 to avoid non-convergence). If the equation fit is degraded (i.e., lower correlation coefficient), then the process stops and the previous value of $\gamma$ is used. This process of determining the coefficients $\alpha_{p,c}$, $\beta_{p,c}$, and $\gamma_{p,c}$ is repeated for each predictor and each class and applied to create the supplemental set of 8 transformed predictors for each class.

Fourteen of the 18 predictors is then used for calibrating the rainfall rate retrieval, with predictors 2 and 3 and their transforms not considered because they are not physically relevant for rain rate retrieval. For each class, each possible pairing of the 14 predictors is regressed against the target rain rates using Eq. (27), and the predictor pair with the highest Pearson correlation coefficient against the target microwave rainfall rates is selected.

As with the rain / no rain discrimination, experiments showed no positive impact from using more than two predictors, again perhaps because of the high degree of correlation among the IR bands for optically thick clouds.

Previous work has shown that the rainfall rates retrieved using this approach generally exhibit a strong systematic dry bias—too wet for low rainfall rates and much too dry for higher rainfall rates. This is believed to be the result of significant scatter in the training data caused by spatial displacements between the coldest cloud tops and the heaviest rainfall rates. To address this problem, an adjustment for the retrieved rainfall rate is derived that adjusts its distribution to match the training microwave rainfall rates.

Specifically, for each rainfall class, the rainfall rates are retrieved using the coefficients derived above, and then are sorted from lowest to highest and matched against the training rainfall rates which have also been independently sorted lowest to highest. The result of this match is a lookup table (LUT) whereby the value of the retrieved rainfall rate is converted to the value of the corresponding microwave rainfall rate so that the distribution of the retrieved rainfall rate will match that of the microwave rainfall rates.

To create a useful LUT, linear interpolation is used to create a table with evenly spaced increments of 0.01 mm/h for the training rainfall rates. In addition, since the MW rainfall rates have a lower dynamic range (in part due to their coarser spatial resolution), but since extrapolation of the data could produce non-physical results, for all values between

50 mm/h (generally the highest rain rate retrieved from MW radiances) and 100 mm/h the input and output values are set equal to one another (i.e., a retrieved rainfall rate of 75 mm/h will be mapped to a final rainfall rate of 75 mm/h). Linear interpolation is then performed between the data point with the highest rainfall rates and the (50 mm/h, 50 mm/h) data point. This LUT is then written to the end of the retrieval coefficient table in Table 4, Section 3.3.2.

### 3.5.5 Application to independent data

The predictors and coefficients obtained during the calibration outlined in the previous two subsections are then applied to the current ABI imagery using Eq. (26) with the appropriate coefficients and predictor values. To avoid the potential data quality issues with any pixel that is missing one but not all bands, if any of the input bands has a value less than 174 K, the value of the 11.2-micron (band 14) brightness temperature is set to the missing value of -999.0. The rain /no rain discriminator is then computed. For values below the threshold, a rain rate of zero is assigned; for values above the threshold, the rainfall rate is computed using Eq. (26) with the rain rate coefficients (and predictor transformations from Eq. (33) as needed), followed by the distribution adjustment.

In order to prevent artifacts at the edges of each 15x15º lat / lon box, for each ABI pixel nine separate rain rate retrievals are computed based on the calibration coefficients for the same cloud types in the 3x3 grid of 15x15º lat / lon boxes centered on the pixel. For example, for a pixel in class 213, rain rates would be retrieved using the coefficients for classes 177, 180, 183, 210, 213, 216, 243, 246, ad 249 (see Fig. 2 for locations). The final rain rate total is the inverse distance weighted average using the cube of the distance between the pixel and the centers of the 15x15º lat / lon box for each contributing class.

Finally, because some or sometimes all of the rainfall at cloud base may evaporate before reading the surface, the mean-layer (lowest third of the model domain) relative humidity (RH) from the NWS / NCEP GFS is used to adjust the rain rates. The adjustment was developed by regressing the difference between the MWCOMB rain rates and the corresponding Stage IV 1-h rainfall accumulations (aggregated onto the MWCOMB grid) against the RH values to derive the following additive adjustment:

$$RR_{add} = RR + 0.115825 * (\max(RH, 61)) - 10.7354 \quad (35)$$

where RR is the additive-adjusted rain rate and RH is the mean-layer RH in percent. The resulting ratios of the MWCOMB rain rates to the additive-adjusted rain rates to the corresponding MW were then regressed against the RH values to derive the following multiplicative adjustment:

$$RR_{mult} = RR_{add} * (0.000112891[\max(RH, 22.32)]^2 - 0.00504012 * [\max(RH, 22.32)] + 0.476117) \quad (36)$$

where $RR_{mult}$ is the rain rate after applying the multiplicative adjustment.

## 3.6 GOES-17 LHP Mitigation

The GOES-17 LHP mitigation imposes the following changes on GOES-17 only:

- Only predictors 2, 3, and 9 are used for rain / no rain discrimination; only predictors 9 and 18 is used for rain rate retrieval. This contingency is needed only in the calibration step since the retrieval step will use only those predictors in the calibration file.
- Since cloud type classification cannot be performed using band 14 only, 110 additional composite classes (numbered 331-440) are created from the matched IR-MWCOMB data by combining data from the three classes in the same 15x15° lat / lon box; e.g., class 331 contains all of the data from classes 1-3 and class 440 contains all of the data from classes 328-330. To avoid redundant storage, the matched data for classes 331-440 is assembled "on the fly" from the component classes during calibration.
- The retrieval step uses only classes 331-440.

## 3.7 Algorithm Output

The final output of this algorithm is the Rainfall Rate product—a field of instantaneous rainfall rates in mm/h (rounded to the nearest integer) at the same resolution as the ABI IR data—2 km at nadir. Note that for output purposes these values are converted to short integers and multiplied by 10, so the effective values in the output files are tenths of mm per hour. This product will also be accompanied by a grid of corresponding quality flags, with values of 0 for good data and non-zero for data that are of questionable quality due to deficiencies in the input data, as described in Table 6:

| Byte | Bit | Flag | Source | Value |
|---|---|---|---|---|
| 0 | 0 | Rainfall Rate output | RR | 1=bad data; 0=OK |
| | 1 | Local zenith angle block-out zone | SDR | 1=local zenith angle>70° or lat>60°; 0=OK |
| | 2 | Bad input data for 1st rain / no rain predictor | SDR and RR | 1=bad data; 0=OK |
| | 3 | Bad input data for 2nd rain / no rain predictor | SDR and RR | 1=bad data; 0=OK |
| | 4 | Bad input data for 1st rain rate predictor | SDR and RR | 1=bad data; 0=OK |
| | 5 | Bad input data for 2nd rain rate predictor | SDR and RR | 1=bad data; 0=OK |
| | 6 | Retrieval coefficients missing | RR | 1=no retrieval coefficients; 0=OK |
| | 7 | FPM temperature > 81.2 K | SDR | 1=yes, 0=no |

**Table 6.** Quality flags for the Rainfall Rate product.

Note that if any of bits 2-6 are set to 1 that all of them should be set to 1.

In addition, two quality information fields will be output: a gridded file containing flags indicating if the rainfall rate values were truncated at 0 mm/h or at 100 mm/h (Table 7) and a gridded file containing the rainfall class (1-330/440) of a particular pixel (Table 8):

| Byte | Bit | Flag | Source | Value |
|---|---|---|---|---|
| 0 | 0 | Rain rate > 100 mm/h | RR | 1=rain rate >100 mm/h but truncated at 100 mm/h;<br>0=rain rate <100 mm/h |
| | 1 | Rain rate < 0 mm/h | RR | 1=rain rate <0 mm/h but truncated at 0 mm/h;<br>0=rain rate >0 mm/h |

**Table 7.** Diagnostic information for the Rainfall Rate product.

| Grid | Field | Source | Value |
|---|---|---|---|
| 1 | Precipitation class identifier | RR | Value of rain class, ranging from 1 to 330 (440 for GOES-17) |

**Table 8.** Gridded quality information for the Rainfall Rate product.

Additional diagnostic information will be provided by the corresponding retrieval coefficient table (Table 4, Section 3.3.2).

# 4 PRODUCT VALIDATION

## 4.1 Validation Period and Ground Validation Data Sets

Two ground validation data sets were chosen and will be described in more detail below: the Multiple Radar Multiple Sensor (MRMS) gauge-adjusted rain rate field, which covers only the CONUS but at very high temporal resolution, and the GPM Dual-frequency Precipitation Radar (DPR) which covers the full-disk equatorward of 63 degrees but only covers a particular area anywhere from twice in a day to every few days depending on latitude.

### 4.1.1 Gauge-adjusted MRMS Rain Rates

MRMS is a composite of US and Canadian radars that are regridded onto a 0.01º lat / lon grid that is refreshed every 2 minutes (Zhang et al. 2016). In addition to the radar-only instantaneous rates, MRMS also produces gridded hourly and multi-hour accumulations that have been adjusted using rain gauge data; however, gauge-adjusted instantaneous rain rates are not currently available. Consequently, the instantaneous rates are multiplied by the ratio of the corresponding gauge-adjusted 1-hour accumulations to the unadjusted 1-hour accumulations.

### 4.1.2 GPM DPR Rain Rates

The GPM instrument package includes the DPR (Iguchi et al. 2010), which scans at both 13.6 GHz (Ku band) and 35.5 GHz (Ka band). The Ku band was selected because of its wider swath (245 km vs. 120 km for the Ka band); even with the wider swath, some locations average less than one overpass per day. Versions 6 and 7 (whichever was most current at the time—no reprocessed data are used) are used for validating the Enterprise rainfall rates.

## 4.2 Reprocessed and Real-Time Output from ABI Data

Ground validation of the Enterprise Rainfall Rate products has been performed using a combination of real-time and retrospective rain rates retrieved at STAR going back to 1 March 2017 (the day the radiances were declared Provisionally validated) for GOES-16 and for 14 September 2018 (the day an error in the co-registration between the midwave IR and longwave IR ABI FPMs was corrected) for GOES-17. To allow the most direct comparison possible and minimize seasonal effects, this version of the ATBD will use validation statistics for the 12-month period ending 31 May 2020.

### 4.2.1 Precision and Accuracy Estimates

The F&PS specifications for the Rainfall Rate algorithm (see Table 1) refer to instantaneous rainfall rates, which is why validation is performed solely against (gauge-adjusted, in the case of MRMS) radar. The paucity of reliable ground-based radar data outside the CONUS and southern Canada makes DPR essential for validation despite its relatively infrequent revisit rate.

Because rainfall rates are highly skewed toward low rates that are of much less hydrometeorological interest than higher rain rates, the F&PS precision spec focuses on the performance of the algorithm for rain rates of 10 mm/h (see Table 1). Specifically, when the rain rate at a given pixel is 10 mm/h, the corresponding observed value should be within 9 mm/h (i.e., within the range of 1 – 19 mm/h) 68% of the time. This appears to be a very loose requirement compared to most products; however, instantaneous rainfall rate is far more variable in both space and time than most other geophysical parameters, and slight displacement errors can make the validation statistics look much worse than what a side-by-side comparison of the imagery to ground validation data might suggest. Because of this, a "fuzzy" approach for fine-scale rainfall validation has been selected whereby the Rainfall Rate pixel is compared with the pixel within a 10-km radius that has the most similar value rather than with the directly corresponding pixel. This is a variant of the "single observation –neighborhood forecast" strategy described in Ebert (2008). However, it is applied only to the accuracy and precision calculations; all other statistical validation (including the scatterplots in the next two sections) directly compare the satellite pixels with the corresponding ground validation data.

#### 4.2.1.1 CONUS Validation against MRMS Q3

Figure 3 shows a scatterplot of the rainfall rates from GOES-17 and GOES-16 during the 12-month validation period with the density of points indicated by color (red=more dense; purple=less dense) to eliminate the visually misleading effect of multiple overlapping points.

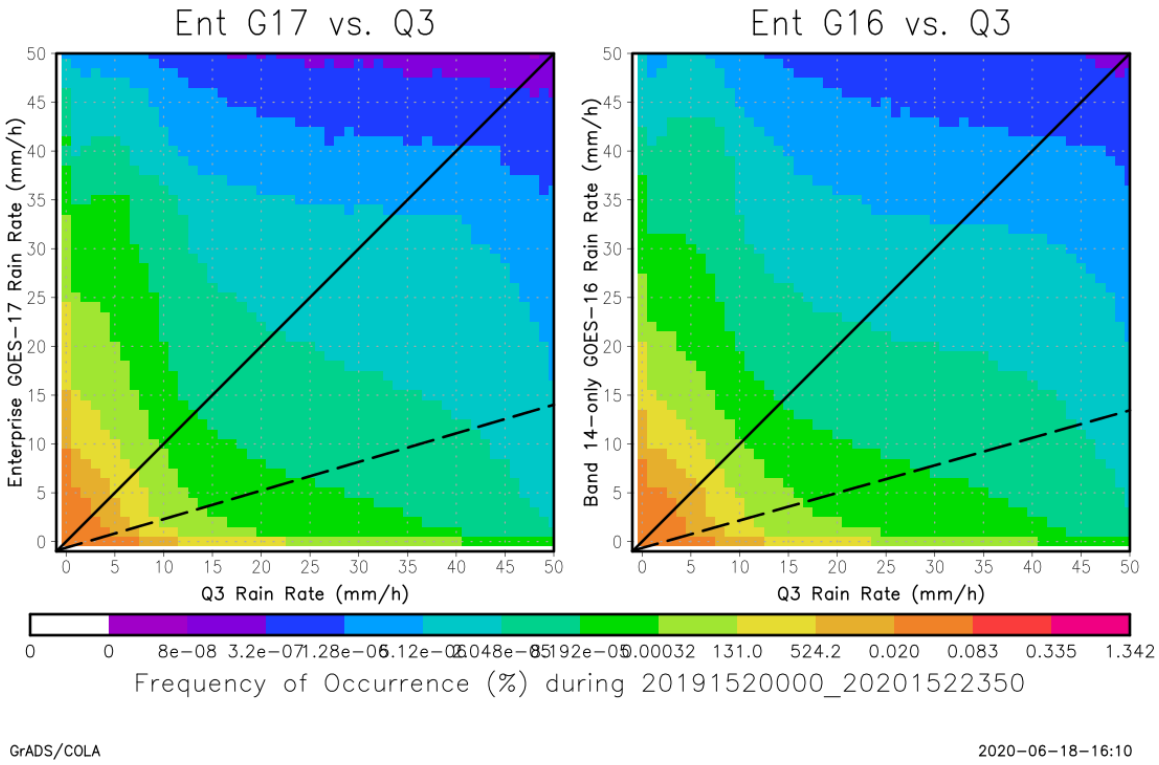


**Figure 3.** Scatterplot of Rainfall Rate algorithm vs. collocated gauge-adjusted MRMS rain rates for 1 June 2019-31 May 2020; colors are related to pixel density with red highest and purpose lowest. Solid line is the 1:1 line and the dashed line is the best-fit line.

Although there is a high degree of scatter (corresponding to a Pearson correlation coefficient of 0.28 for GOES-17 and 0.32 for GOES-16), some of it can be attributed to small horizontal displacements between the satellite cloud tops and the ground-level rainfall because vertical shear will cause the hydrometeors to fall at an angle from the vertical, and at a 2-km spatial resolution this effect can be quite noticeable. Regardless, there is a significant systematic dry bias; i.e., the higher rain rates are underestimated by the satellite.

The performance of the algorithm against the F&PS precision spec is illustrated in Fig. 4 by the cumulative distribution function (CDF) of absolute error in the Rainfall Rate product (the values along the abscissa) with respect to the gauge-adjusted MRMS for only those pixels with algorithm values between 9.5 and 10.5 mm/h (there are too few pixels with rain rates of exactly 10.0 mm/h to enable a statistically significant analysis). These errors were computed using the "fuzzy" verification strategy described in Section 4.2.1. The dashed line indicates that 68% of the GOES-16 errors are below 7.8 mm/h, which is within the spec value of 9.0 mm/h; however, for GOES-17 the 68$^{th}$ percentile of absolute error is at 9.4 mm/h, which does not meet spec. This is a result of the LHP issues and the necessary mitigation that have been described previously.

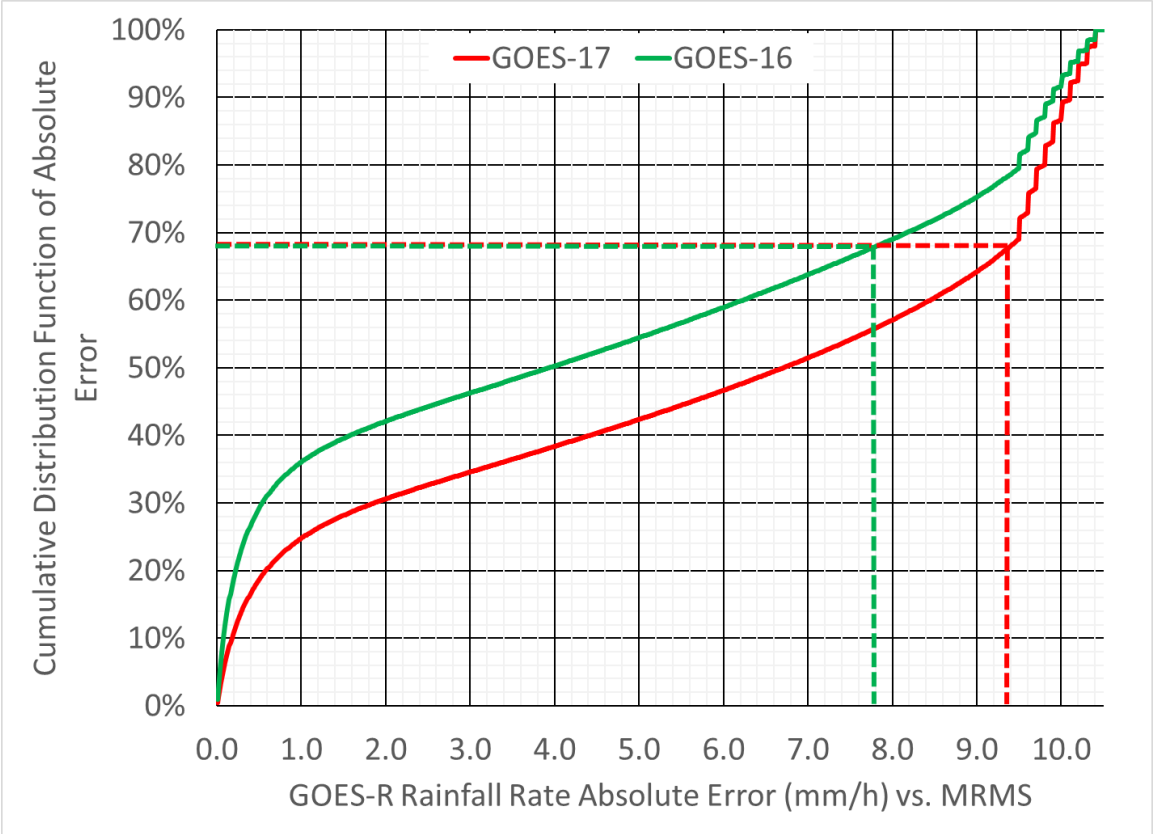


**Figure 4.** CDF of errors of Rainfall Rate product with rates of 9.5-10.5 mm/h vs. gauge-adjusted MRMS.

Examining the spatial variability of accuracy and precision vs. gauge-adjusted MRMS over the CONUS in Figure 5 sheds additional light on why the GOES-17 performs significantly worse than the GOES-16 rain rates.

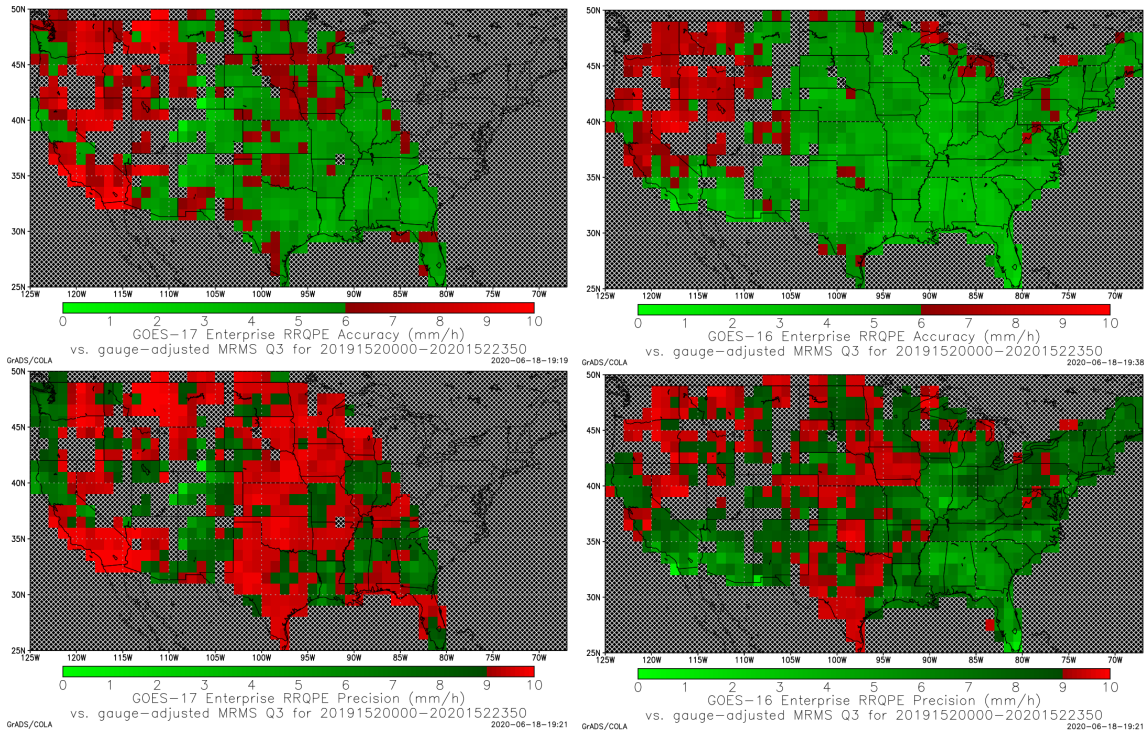


**Figure 5.** Accuracy (top row) and precision (bottom row) vs. gauge-adjusted MRMS for the GOES-R Rainfall Rate product for GOES-17 (left column) and GOES-16 (right column) for 1 June 2019 - 31 May 2020. Green shading indicates where spec is met, red where it is not.

The rainfall rates tend to be most skillful over the southeastern United States, which will degrade the statistics for GOES-17 since that region represented as well in the validation data as for GOES-16. However, in regions where they overlap, the GOES-16 rain rates still tend to be more accurate—even along 106$^{th}$ meridian which represents the approximate center point between the two (and hence where the view angle is roughly the same for both instruments. This demonstrates the compromise of performance that was made to produce non-noisy estimates of rainfall from the excessively warm GOES-17 ABI.

### 4.2.1.2 Validation against GPM DPR

As with MRMS, validation against GPM DPR for the 12 months ending 31 May 2020 are shown in this section, albeit with global coverage rather than CONUS coverage.

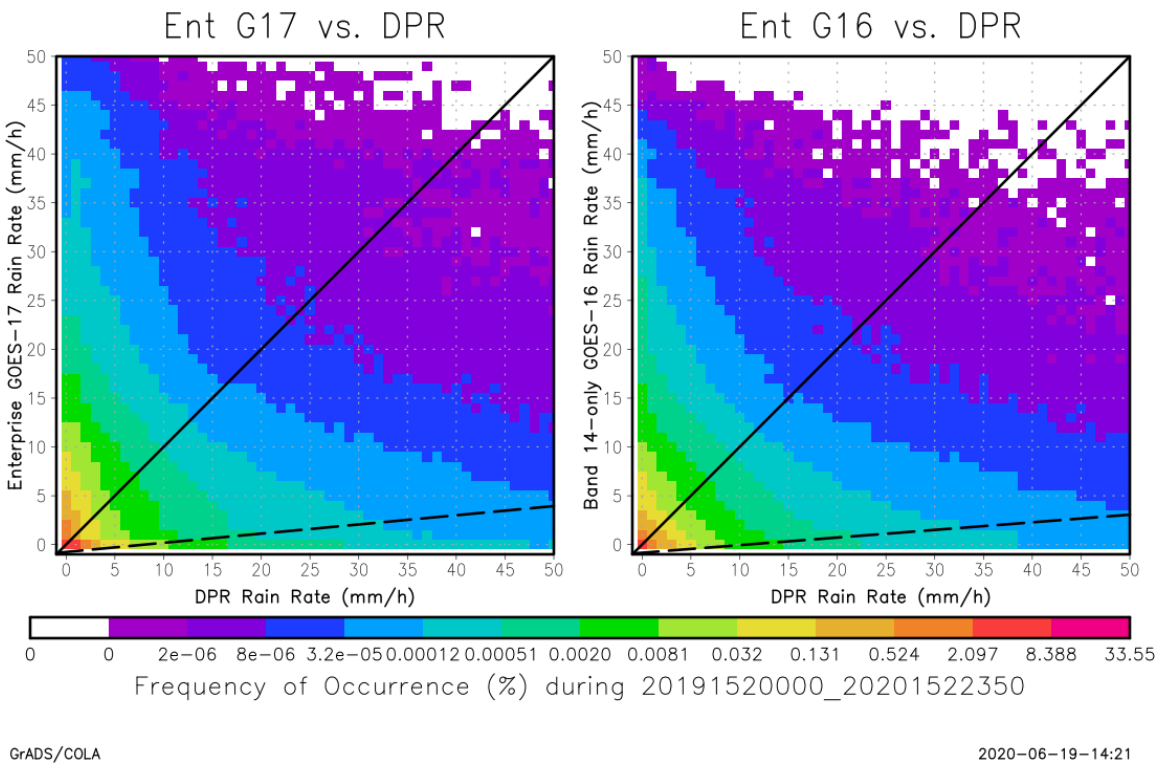


**Figure 6.** Scatterplot of Rainfall Rate algorithm vs. collocated GPM DPR rain rates for 1 June 2019-31 May 2020; colors are related to pixel density with red highest and purpose lowest. Solid line is the 1:1 line and the dashed line is the best-fit line.

As the scatterplot in Figure 6 shows, the degree of scatter between the GOES rain rates and the GPM DPR rain rates is even greater than with MRMS, with a Pearson correlation coefficient of 0.170 for GOES-17 and 0.127 for GOES-16. However, the algorithm with an accuracy of accuracy of 5.91 mm/h and 5.21 mm/h for GOES-17 and -16, respectively (spec is 6.00 mm/h), and a precision of 8.96 mm/h and 8.69 mm/h for GOES-17 and -16, respectively (spec is 9.00 mm/h).

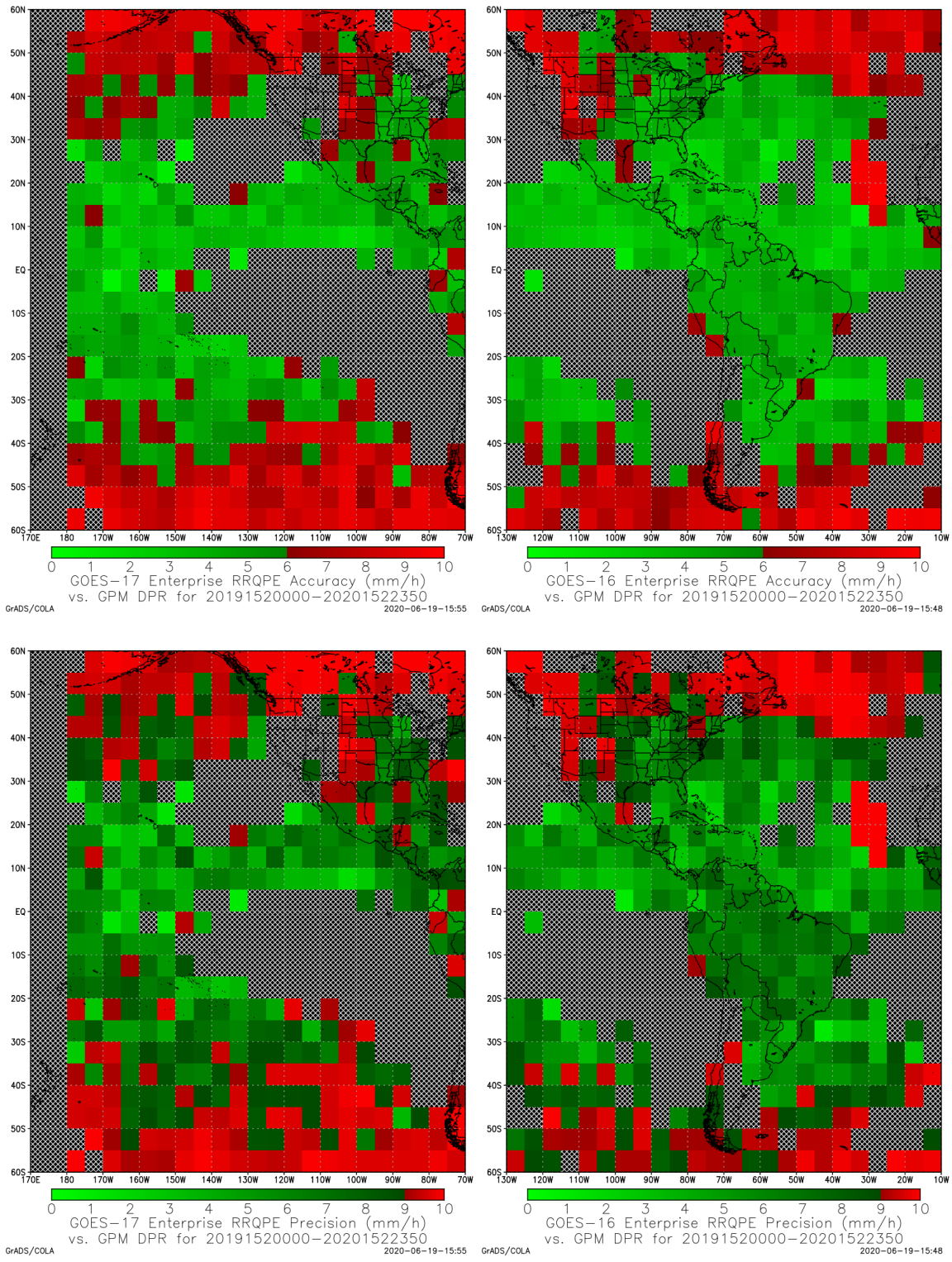


**Figure 7.** Accuracy (top row) and precision (bottom row) vs. GPM DPR for the GOES-R Rainfall Rate product for GOES-17 (left column) and GOES-16 (right column) for 1 June 2019 - 31 May 2020. Green shading indicates where spec is met, red where it is not.

As Figure 7 shows, the algorithm does best in the tropics and worse in the higher latitudes, as one would expect given the preponderance of convective rainfall in the former and stratiform rainfall in the latter. It is also clear that GOES-16 rain rates have less error and bias than GOES-17 in the regions where they overlap, which is also expected since the GOES-17 rain rates are retrieved using only ABI band 14 to mitigate the FPM cooling issue.

### 4.2.2 Error Budget

The validation of retrieved rain rates from GOES-16 and -17 against gauge-adjusted MRMS and DPR for 1 June 2019 through 31 May 2020 is summarized in Table 9 using the "fuzzy" verification described in Section 4.2.1. As discussed in Sections 4.2.1.1 and 4.2.1.2, the precision and accuracy specs are met in all cases except for GOES-17 vs. MRMS over the CONUS, and part of that is because the validation statistics there are weighted heavily toward the western CONUS where orographic effects degrade the skill of the estimates.

| **Ground Validation (coverage)** | **Accuracy (mm/h) at 10 mm/h** | | **Precision (mm/h) at 10 mm/h** | | **Number of data points** | |
|---|---|---|---|---|---|---|
| | **GOES-17** | **GOES-16** | **GOES-17** | **GOES-16** | **GOES-17** | **GOES-16** |
| MRMS (CONUS) | 5.50 | 4.36 | 9.39 | 7.81 | 6,867,843 | 11,201,180 |
| DPR (FD) | 5.91 | 5.21 | 8.96 | 8.69 | 347,934 | 161,680 |
| **F&PS** | **6.0** | | **9.0** | | **-----** | |

**Table 9.** Comparison of Rainfall Rate algorithm validation with F&PS.

# 5 PRACTICAL CONSIDERATIONS

## 5.1 Numerical Computation Considerations

The calibration portion of the algorithm creates / updates a series of external files containing matched MW rainfall rates and ABI predictors, and whenever a file is updated, ingests the data into an array and uses L-U (Lower-Upper) matrix decomposition to solve the resulting matrix for calibration coefficients (Eq. 27) and predictor ID's that are stored in a separate external file. The retrieval portion of the algorithm ingests the calibration coefficient files and the ABI predictor fields that are indicated within these files and applies the coefficient files to the predictor fields, resulting in a rainfall rate field on the same grid as the ABI predictors.

The MW-IR matching, calibration and retrieval portions of the Rainfall Rate Algorithm do not need to be run sequentially; in fact, parallel processing is preferred as long as care is taken to make sure that coefficient files are available whenever needed for the retrieval portion of the algorithm. The only stipulation is that for optimal accuracy the calibration should be updated as frequently as new ABI-MW rain rate matchups are available. Since

the MWCOMB data may have a latency of 15 hours, previous ABI data will need to be available for calibration purposes.

## 5.2 Programming and Procedural Considerations

The Rainfall Rate Algorithm requires knowledge of spatial uniformity metrics that are computed for each pixel using pixels that surround it, and also requires an 11x11-pixel window to compute cloud type. Beyond this reliance, the Rainfall Rate Algorithm is purely a pixel by pixel algorithm; no information from previous time periods is required for the retrieval step (though it is needed for the calibration step—see below). No temporal averaging is performed to generate the 10-min products; the most recently available ABI image is used to generate the current Rainfall Rate product.

A collection of MWCOMB rainfall rates during the previous 2-3 days should be available for use as calibration targets. However, if necessary the rainfall rate algorithm can run using pre-computed calibration coefficients which will be adjusted whenever target MWCOMB rainfall rates become available and a sufficient supply of matched data pairs has thus been built up. Furthermore, if the availability of MWCOMB rainfall rates is interrupted, the algorithm will continue to produce estimates using the most recently computed calibration coefficients.

## 5.3 Quality Assessment and Diagnostics

Quality flags will be produced and provided along with the rainfall rate fields, with non-zero values for pixels whose inputs have values outside the acceptable range. These flags are described in detail in Section 3.7. Table 10 lists acceptable range values for the inputs. Note that the minimum values in the table are for computational purposes: values lower than that would produce negative predictor values, which will in turn result in errors when the nonlinear predictor transformation described in Section 3.5.2 is performed.

| Input ID | Predictor Description | Minimum Value |
|---|---|---|
| 1 | $T_{6.2}$ | 174 K |
| 2 | $S=0.568*(T_{min,11.2}-217\ K)$ | -25 K |
| 3 | $T_{avg,11.2}-T_{min,11.2}-S$ | -85 K |
| 4 | $T_{7.34}-T_{6.19}$ | -10 K |
| 5 | $T_{8.5}-T_{7.34}$ | -10 K |
| 6 | $T_{11.2}-T_{7.34}$ | -40 K |
| 7 | $T_{8.5}-T_{11.2}$ | -25 K |
| 8 | $T_{11.2}-T_{12.3}$ | -15 K |
| 9 | $T_{11.2}$ | 174 K |

**Table 10.** Minimum acceptable values for each algorithm predictor.

The following procedures are recommended for diagnosing the performance of the rainfall retrieval algorithm.

- Periodically image the individual test results to manually identify artifacts or non-physical behaviors.

- Automatically compute performance statistics for the algorithm (preferably daily) against DPR and gauge-adjusted MRMS and note any significant deviations from typical values.

## 5.4 Exception Handling

The Rainfall Rate Algorithm includes checking the validity of each input ABI band before retrieving a rainfall rate, and a 'missing' (-999.0) value is assigned to a pixel if any of the input values are outside the acceptable range. A missing value is also assigned to that pixel if the calibration coefficients are not available for any of the 9 15x15° lat / lon calibration boxes that contribute to that pixel; this is done by checking the first rain detection predictor ID, the Heidke Skill Score, and the correlation coefficient from the training file for missing values. The bits 1-4 (depending on the predictor; see Table 6 in Section 3.7) of the quality flag for that pixel will also be set to 1. Note that it is possible for bits 1-4 to be set to 1 even when there is a non-missing rain rate at a particular pixel; this simply means that the calibration coefficients were not available for the 15x15° lat / lon box containing the pixel and that the rain rate therein was retrieved using some of the neighboring 15x15° boxes only. The Rainfall Rate Algorithm also expects the Level 1b processing to flag any pixels with missing geolocation or viewing geometry information.

If the MWCOMB data are unavailable, the algorithm will continue to produce estimates of rain rate using the most recently available calibration coefficient tables; performance will degrade slightly as a result but the degradation will be limited. If one or more individual ABI bands used by the algorithm become unavailable, the algorithm will first output missing values (and corresponding quality flags) for any pixels that use the missing ABI band, and then subsequent updates to the calibration coefficients will ignore the missing bands and retrieval will continue as normal. The degree of degradation in performance will depend on the band(s) that are lost.

## 5.5 Algorithm Validation

In addition to the validation described in Section 4, validation statistics compared to the previous 24 hours of gauge-adjusted and MRMS data are automatically generated daily at STAR. Spatial plots of the rain rates and also of the errors in rain rates compared to gauge-adjusted MRMS are also created daily and examined at STAR.

# 6 ASSUMPTIONS AND LIMITATIONS

This section describes the assumptions and limitations of the current version of the Rainfall Rate Algorithm.

## 6.1 Performance

Several assumptions have been made in developing and estimating the performance of the Rainfall Rate Algorithm. They are listed below, accompanied by proposed mitigation strategies in parentheses.

1. The calibration target (MWCOMB) rainfall rates are accurate. (No mitigation possible.)

2. The calibration target rainfall rates are available with a reasonably short lag time. Note that in the absence of calibration data, the algorithm will continue to produce retrievals based on the last available set of calibration coefficients, though with some degradation of performance. (No mitigation possible, but see Section 6.3.1.)

3. The parallax adjustment of the ABI pixels is accurate. (Refinement of the parallax scheme is possible but not a high enough priority to pursue at this time.)

4. Limb cooling is sufficiently uniform in each 15x15º calibration box to not require adjustment. (Limb cooling adjustments require knowledge of the atmospheric water vapor content along the path length. For window bands the effects of water vapor are small enough that a climatological adjustment is sufficient, and this is used when estimating the cloud-top temperature from band 14. However, limb cooling adjustments for WV absorption bands are much more challenging and are not being pursued at this time.)

5. The available validation data (DPR and gauge-adjusted MRMS) are sufficiently accurate and provide a sufficiently representative sample to evaluating whether the algorithm meets spec. (No mitigation possible.)

6. The processing system allows for processing of multiple pixels at once for application of the spatial uniformity tests and calculation of the pixel type. (No mitigation possible)

7. Striping (i.e., when two or more detectors have slightly different calibrations, producing scan lines that are biased with respect to one another) and spectral shifts are minimal. (No mitigation possible)

8. No data aggregation is performed in time; i.e., if the frequency of ABI imagery exceeds the product refresh rate, only one ABI image will be processed per product. (No mitigation possible)

In addition, a number of limitations in the ability to retrieve rainfall rates from satellite data have been identified and are listed here.

1. Satellite-based rainfall algorithms generally exhibit much better skill for convective (warm-season) rainfall than for stratiform (cold-season) rainfall, because the relationship between cloud-top temperature and rainfall rate is much stronger for the former than the latter. The inclusion of additional ABI bands provides some mitigation by implicitly including information about cloud-top properties (particle size and phase).

2. The current version of the algorithm does not account for modulation of rainfall by topography. The effects of orography on precipitation are highly complex and the published efforts that are centered on calculation of upslope / downslope flow near topography produce results that look realistic but do not significantly enhance skill when validated against ground data.

## 6.2 Assumed Sensor Performance

It is assumed that the sensor will meet its current specifications. However, the Rainfall Rate Algorithm will be dependent on the following instrumental characteristics.

- The spatial variation predictors in the Rainfall Rate Algorithm will be critically dependent on the amount of striping in the data. Note that this will affect the retrieval only when any texture-related predictors are among the selected predictors selected by the algorithm.

- Unknown spectral shifts in some channels will affect the BTD calculations and thus compromise some of the predictors. Note that this will affect the retrieval only when any BTD's are among the predictors selected by the algorithm.

- Any noise in the data (e.g., from an insufficiently cooled FPM) is exacerbated in the BTDs and can make the BTDs too noisy to use even when the noise for individual bands is relatively tolerable.

## 6.3 Pre-Planned Product Improvements

A number of potential improvements are being in progress or being considered for evaluation:

### 6.3.1 Direct Matching of IR with MW Rain Rates

Since the MWCOMB product re-grids the MW footprints onto a lat / lon grid and does not contain time information (i.e., when the overpass occurred during each half hour), a process is being developed to directly match the IR predictors with operational MW rain rates retrieved using the Microwave Integrated Retrieval System (Iturbude-Sanchez et al. 2011) instead of using MWCOMB. Rain rates will be used from the Global Precipitation Mission (GPM) Microwave Imager (GMI), the Advanced Microwave Sounding Unit-B / Microwave Humidity Sensor (AMSU-B/MHS), the Special Sensor Microwave Imager

Sounder (SSMIS), and the Advanced Microwave Scanning Radiometer-2 (AMSR2). Other MW instruments will be added as MIRS rain rates become available.

### 6.3.2 Incorporation of Geostationary Lightning Mapper (GLM) Data

Experiments with incorporating GLM fields of Flash Extent Density and Average Flash Area that have been remapped to the ABI grid have shown a positive impact on performance, particularly for GOES-17. Additional work with longer time periods of data is ongoing to confirm the impacts; once confirmed, appropriate changes will be made to the operational algorithm.

# 7 REFERENCES


Ba, M., and A. Gruber, 2001: GOES Multispectral Rainfall Algorithm (GMSRA). J. Appl. Meteor., 40, 1500-1514.

Ebert, E. E., 2008: Fuzzy verification of high-resolution gridded forecasts: A review and proposed framework. *Meteor. Appl*., **15**, 51-64.

Iguchi, T., S. Shinta, R. Menghini, N. Yoshida, J. Awaka, M. Le, V. Chandrasekar, and T. Kubota, 2010: GPM/DPR Level-2. Algorithm Theoretical Basis Doc., 68 pp., https://pps.gsfc.nasa.gov/atbd.html.

Iturbide-Sanchez, F., S. A. Boukabara, R. Y. Chen, K. Garrett, C. Grassotti, W. C. Chen, and F. Z. Weng, 2011. Assessment of a variational inversion system for rainfall rate over land and water surfaces. *IEEE Trans. Geosci. Remote Sens*., **49**, 3311-3333.

Joyce, R. J., J. E. Janowiak, and G. Huffman, 2001: Latitudinally and seasonally dependent zenith-angle corrections for geostationary satellite IR brightness temperatures. *J. Appl. Meteor*., **40**, 689-703.

-----, -----, P. A. Arkin, and P. Xie, 2004a: CMORPH: A method that produces global precipitation estimates from passive microwave and infrared data at high spatial and temporal resolution. *J. Hydrometeor*., **5**, 487-503.

Kuligowski, R. J., 2002: A self-calibrating real-time GOES rainfall algorithm for short-term rainfall estimation. *J. Hydrometeor*., **3**, 112-130.

-----, Y. Li, and Y. Zhang, 2013: Impact of TRMM data on a low-latency, high-resolution precipitation algorithm for flash-flood forecasting. *J. Appl. Meteor. Cli*., **52**, 1379-1393.

-----, -----, Y. Hao, and Y. Zhang, 2016: Improvements to the GOES-R rainfall rate algorithm. *J. Hydrometeor*, **17**, 1693-1704.

Olson, W. S., C. D. Kummerow, S. Yang, G. W. Petty, W. K. Tao, T. L. Bell, S. E. Lang, D. E. Johnson, and C. Chiu, 2006: Precipitation and latent heating distributions from satellite passive microwave radiometry. Part I: Improved method and uncertainties. *J. Appl. Meteor. Cli*., 45, 702-720.

Vicente, G. A., J. C. Davenport, and R. A. Scofield, 2002: The role of orographic and parallax corrections on real time high resolution satellite rainfall rate distribution. *Int. J. Remote Sens*., **23(2)**, 221-230.

Zhang J., and coauthors, 2016: Multi-Radar Multi-Sensor (MRMS) Quantitative Precipitation Estimation: Initial operating capabilities. *Bull. Amer. Meteor. Soc*., **97**, 621–638.